

Article pubs.acs.org/JCTC

# Reduced-Order Modeling Approach for Electron Transport in **Molecular Junctions**

Weiqi Chu\* and Xiantao Li\*



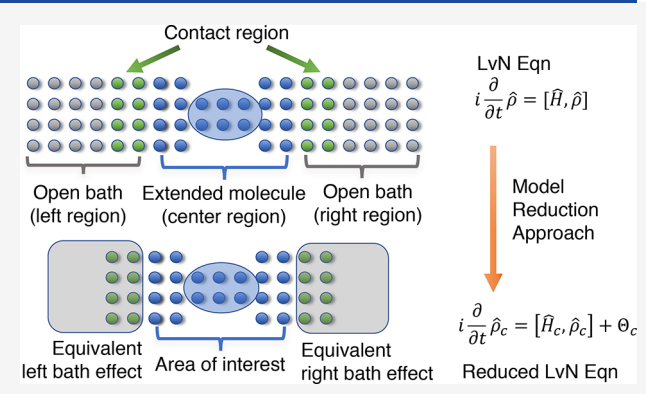
Cite This: https://dx.doi.org/10.1021/acs.jctc.9b01090



**ACCESS** 



ABSTRACT: To describe nonequilibrium transport processes in a quantum device with infinite baths, we propose to formulate the problems as a reduced-order problem. Starting with the Liouville-von Neumann equation for the density-matrix, the reduced-order technique yields a finite system with open boundary conditions. We show that with appropriate choices of subspaces, the reduced model can be obtained systematically from the Petrov-Galerkin projection. The self-energy associated with the bath emerges naturally. The results from the numerical experiments indicate that the reduced models are able to capture both the transient and steady states.



Article Recommendations

### 1. INTRODUCTION

In the past decades, there has been significant progress in the investigation of molecular electronics and quantum mechanical transport, 1-3 one emerging issue among which is the modeling of interfaces or junctions between molecular entities.<sup>4–7</sup> The junctions encompass two sections: (i) a molecular core at the nanometer scale that bridges two metallic devices and (ii) the surrounding areas from contacting materials. Notable examples include quantum dots, quantum wires, and molecule-lead conjunctions. The junctions play an essential role in determining the functionality and properties of the entire device and structure, such as photovoltaic cells, <sup>8,9</sup> intra-molecular vibrational relaxation, <sup>10–13</sup> infrared chromophore spectroscopy, and photochemistry. <sup>14–17</sup> At such a small spatial and temporal scale, modeling the transport properties and processes demands a quantum theory that directly targets the electronic structures.

Such problems have been traditionally treated with the Landauer-Büttiker formalism,  $^{18-20}$  which aims at computing the steady-state of a system interacting with two or more macroscopic electrodes, and the nonequilibrium Green's function (NEGF) approach, which, often based on the tightbinding (TB) representation, can naturally incorporate the external potential and predict the steady-state current.<sup>21</sup> This approach was later extended to the first-principle level<sup>22-24</sup> using the density-functional theory (DFT). 25,26

Due to the dynamic nature and the involvement of electron excitations, one natural computational framework for transport problems is the time-dependent density-functional theory (TDDFT),<sup>27-31</sup> which extends the DFT to model electron dynamics. This effort was initiated by Stefanucci and Almbladh<sup>29,32</sup> and Kurth et al.,<sup>27</sup> where the wave functions are projected into the center and bath regions. An algorithm was developed to propagate the wave functions confined to the center region so that the influence from the bath is taken into account. This is later treated by using the complex absorbing potential (CAP) method<sup>33</sup> by Varga.<sup>34</sup> One computational challenge from this framework is the computation of the initial eigenstates. Kurth et al.<sup>27</sup> addressed this issue by diagonalizing the Green's function. However, the normalization is still nontrivial, since the wave functions also have components in the bath regions. Another issue is that the CAP method is usually developed for constant external potentials. For timedependent scalar potentials, a gauge transformation is usually needed to express the absorbing boundary condition,<sup>35</sup> and it is not yet clear how this can be implemented within CAP.

Another framework is based on the Liouville-von Neumann (LvN) equation<sup>36,37</sup> to compute the density-matrix operator directly. One advantage of the LvN approach is that the initial density-matrix can be obtained quite easily from the Green's function. Therefore, diagonalization and normalization are not needed. To incorporate the influence of the bath, the LvN equation has been modified by adding a driving term at the

Received: October 31, 2019 Published: April 24, 2020



contact regions according to the potential bias. This approach was later extended by Zelovich and co-workers, <sup>38–40</sup> which is again motivated by the CAP method. The heuristic derivation in ref 38 starts with the LvN equation, supplemented with an absorbing potential to mimic electron absorption, and then in the anticommutator, the time-dependent density-matrix in the leads are replaced by the corresponding equilibrium density-matrix. This approach was later extended in ref 40 where the empirical driving rates are replaced by state-dependent broadening factors that can be computed from the self-energy of the leads.

This paper follows the density-matrix-based framework. Compared to the driven LvN approach by Sánchez et al., 36 and subsequent works where the LvN equation is modified by adding a driven term that is proportional to the deviation of a target density, we derive the open quantum system using the reduced-order techniques that have been widely successful in many engineering applications.<sup>41–43</sup> We first formulate the full quantum system as a large-dimensional dynamical system with low-dimensional input and output. This motivates a subspace projection approach, which has been the most robust method in reduced-order modeling. 41,42 In particular, we employ the Petrov-Galerkin projection, a standard tool in numerical computations, e.g., linear systems, eigenvalue problems, matrix equations, and partial differential equations (PDEs).44-47 With appropriate choices of the subspaces, we obtain a reduced LvN equation, modeling an open quantum system where the computational domain only consists of the center and contact regions. We illustrate the procedure for a one-dimensional model system, as a first step to treat more realistic systems. The numerical results have shown that the reduced LvN equations can capture both the transient and the steady state

The rest of the paper is organized as follows. In Section 2, we provide a detailed account of our methodology, including the mathematical framework and the derivation of the reduced models. In Section 3, we present results from some numerical experiments to examine the effectiveness of the derived models. Section 4 summarizes the methodology and provides an outlook of future works.

### 2. METHODS AND ALGORITHMS

**2.1. Density-Matrix Formulation.** Following the conventions from existing literature,  $^{24,27,38,39}$  we consider a molecular junction, where a molecule is connected to two semi-infinite leads. More specifically, the physical domain for the entire system is denoted by  $\Omega_{\text{c}}$ , divided into three parts,  $\Omega_{\text{L}}$ ,  $\Omega_{\text{C}}$ , and  $\Omega_{\text{R}}$  representing the left lead, the center region, and the right lead, respectively, as illustrated in Figure 1.

We will start with the LvN equation, which for molecular conduction problems, has been proposed and implemented in a series of papers. The LvN equation governs the dynamics of the density-matrix operator  $\hat{\rho}$ , which can be

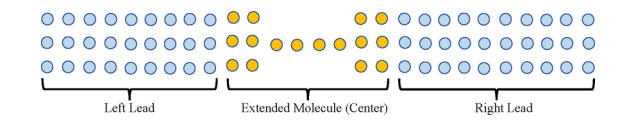


**Figure 1.** Schematic representation of a two semi-infinite lead junction model consisting of two semi-infinite leads: left lead (L), right lead (R), and an extended molecule (C) in the center.

connected to the wave functions (e.g., the Kohn-Sham orbitals) as follows,

$$\hat{\rho}(\mathbf{r}, \mathbf{r}', t) = \sum_{j} n_{j} \hat{\psi}_{j}(\mathbf{r}, t) \hat{\psi}_{j}(\mathbf{r}', t)^{*}$$
(1)

with  $n_j$  being the occupation numbers. The equation can be derived from a time-dependent Schrödinger equation (TDSE), and for the entire system  $\Omega$ , it can be written as,

$$i\partial_t \hat{\rho}(t) = \hat{H}(t)\hat{\rho}(t) - \hat{\rho}(t)\hat{H}(t) = [\hat{H}(t), \hat{\rho}(t)] \tag{2}$$

where the bracket is the general quantum commutator,  $[\hat{A}, \hat{B}] := \hat{A}^* \hat{B} - \hat{B}^* \hat{A}$ , and  $A^*$  denotes the conjugate transpose (or Hermitian transpose of A). Notice that with this generalization, A or B can be non-Hermitian.

Our goal is to derive an open quantum system for the density-matrix at the center region  $\Omega_{C}$ , where the influence from the leads is implicitly incorporated. For convenience, we first assume that the entire system (2) has been appropriately discretized in real (geographic) space  $\Omega$  so that  $\rho(r, r', t)$  is a matrix defined at certain grid points, here denoted by  $\Omega_{\Delta}$  with  $\Delta$  indicating the grid size. Namely,  $\rho(r, r', t)$  is the densitymatrix with  $r, r' \in \Omega_{\Delta}$ . The representation in real space can be obtained through finite-difference, finite-element, or wavelet methods,<sup>48</sup> where the derivatives in the kinetic energy is approximated by local Taylor expansions or via weak formulations. As a result, one arrives at a matrix-valued infinite-dimensional system, and hence, we will drop the ^ notation from now on. Another important class of approximations is tight-binding, where the wave functions are projected to atomic-centered orbitals, in which case, the LvN equation would contain the overlap matrix on the left-hand side when the basis functions are not orthogonal. 39,40,49,50 In this paper, we choose a simple TB Hamiltonian as an intuitive example to illustrate the derivations. This lays the groundwork to treat more general electronic-structure calculation methods. In principle, the reduction method is applicable to any singleparticle Hamiltonian description of the system.

Following the setup by Cini,<sup>21</sup> we treat the problem as an initial value problem (IVP), starting with an initial density  $\rho_0 = f_{\rm eq}(\mu - H_0)$  as an equilibrium density at t = 0. Such setup is particularly amenable for numerical computations. While it is challenging to compute the wave function in a subdomain, which in general requires solving nonlinear eigenvalue problems and normalization,<sup>51</sup> efficient algorithms are available to calculate the density-matrix in a subdomain.<sup>52–54</sup> These algorithms take advantage of the relation between the density-matrix and the Green's function,

$$\rho = \frac{1}{2\pi i} \oint_{C} G(z) dz, \quad G(z) = (zI - H)^{-1}$$
(3)

where the contour encloses all the occupied states. The restrictions of the density-matrix to a finite subdomain can be obtained by  $E^*\rho E$ , where the operator E, with proper arrangement, can be written simply as  $E^*=[I,\,0]$ , with the identity operator I corresponding to the subdomain and the zero matrix corresponding to the exterior (bath). This observation, together with (3), reduces the problem to the computation of the following expression that we have slightly generalized the linear algebraic system to,

$$[\times 0](zI - H)^{-1} \begin{bmatrix} \times \\ 0 \end{bmatrix} \tag{4}$$

where the left and right vectors have finite supports. Namely, the nonzero entries are denoted by × in vectors. Although this amounts to solving an infinite-dimensional linear system, a finite number of unknowns are needed due to the multiplication by the sparse vector on the left and right. The number of nonzero elements in the vectors is related to the size of the center domain and far less than the degrees of freedom in the bath. For one-dimensional (or quasi one-dimensional) systems, an iterative scheme can be used<sup>55,56</sup> to invert the block tridiagonal matrix. For multidimensional problems, a discrete boundary element method<sup>57</sup> can be used.<sup>58</sup> We will refer to these algorithms in general as selective inversion.<sup>53</sup>

Although our model works with the density-matrix, our primary interest is in the electric current induced by a timedependent external potential that is switched on at  $t = 0_+$ . Similar to the theory of linear response,  $^{59-61}$  we consider H(t)as a deviation from its initial value  $H_0$  and write  $H(t) = H_0 +$  $\delta H(t)$  with  $\delta H(t)$  being the applied potential from the leads. The response of the system due to the external potential could be represented in terms of the perturbed density,

$$\delta\rho(t) = \rho(t) - \rho_0, \quad \delta\rho(0) = 0 \tag{5}$$

which satisfies a response equation,

$$i \frac{\mathrm{d}}{\mathrm{d}t} \delta \rho(t) = [H(t), \delta \rho(t)] + \Theta(t)$$
 (6)

Here the nonhomogeneous term  $\Theta(t)$ ,

$$\Theta(t) = [\delta H(t), \rho_0] \tag{7}$$

incorporates the influence from the external potential.

As is customary, <sup>27,36,38,62</sup> we neglect the direct coupling between the two leads and partition the density-matrix and the

Hamiltonian operator in accordance with the partition of the domain indicated in Figure 1. Here we use the subscripts L, R to denote the left, right lead domains and C to denote the extended molecule part in the center. For example,  $H_{\rm CC}$  is the restriction of Hamiltonian in the center domain  $\Omega_{\rm C}$ . According to the previous partition, eq 6 can be translated to a more transparent block-wise form,

$$i \frac{\mathrm{d}}{\mathrm{d}t} \begin{pmatrix} \delta \rho_{\mathrm{LL}} & \delta \rho_{\mathrm{LC}} & \delta \rho_{\mathrm{LR}} \\ \delta \rho_{\mathrm{CL}} & \delta \rho_{\mathrm{CC}} & \delta \rho_{\mathrm{CR}} \\ \delta \rho_{\mathrm{RL}} & \delta \rho_{\mathrm{RC}} & \delta \rho_{\mathrm{RR}} \end{pmatrix}$$

$$= \begin{bmatrix} H_{\mathrm{LL}} & H_{\mathrm{LC}} & 0 \\ H_{\mathrm{CL}} & H_{\mathrm{CC}} & H_{\mathrm{CR}} \\ 0 & H_{\mathrm{RC}} & H_{\mathrm{RR}} \end{pmatrix}, \begin{pmatrix} \delta \rho_{\mathrm{LL}} & \delta \rho_{\mathrm{LC}} & \delta \rho_{\mathrm{LR}} \\ \delta \rho_{\mathrm{CL}} & \delta \rho_{\mathrm{CC}} & \delta \rho_{\mathrm{CR}} \\ \delta \rho_{\mathrm{RL}} & \delta \rho_{\mathrm{RC}} & \delta \rho_{\mathrm{RR}} \end{pmatrix} + \Theta$$
(8)

We are interested in the case when  $\delta H$  corresponds to scalar potentials in the leads, denoted by  $U_{\rm L}(t)$  and  $U_{\rm R}(t)$ , and  $\delta H$ writes as a diagonal matrix in the form

$$\delta H(t) = \begin{pmatrix} U_{\rm L}(t)I_{\rm L} & 0 & 0\\ 0 & 0 & 0\\ 0 & 0 & U_{\rm R}(t)I_{\rm R} \end{pmatrix} \tag{9}$$

where  $I_{\rm L/R}$  are identity matrices of size  $n_{\rm L/R}$ . Direct computations from (eq 7) yield that the matrix function  $\Theta(t)$  follows

$$\Theta(t) = \begin{bmatrix} 0 & U_{\rm L}(t)\rho_{\rm LC}(0) & (U_{\rm L}(t) - U_{\rm R}(t))\rho_{\rm LR}(0) \\ - U_{\rm L}(t)\rho_{\rm CL}(0) & 0 & - U_{\rm R}(t)\rho_{\rm CR}(0) \\ - (U_{\rm L}(t) - U_{\rm R}(t))\rho_{\rm RL}(0) & U_{\rm R}(t)\rho_{\rm RC}(0) & 0 \end{bmatrix}$$

$$(10)$$

In practice, to mimic the infinite leads, one has to pick much larger regions  $\Omega_{L/R}$  to prevent the finite size effect, e.g., a recurrence. This makes a direct implementation using eq 8 impractical and demands tremendous computational cost to simulate the bath environment modeled by two leads. An appropriate reduction is needed to reduce the complexity of the full problem and provide equations of much less degrees of freedom that describe and predict the properties of the center region exclusively. This can be done by eliminating the semiinfinite blocks  $\delta \rho_{\rm LL}$  and  $\delta \rho_{\rm RR}$  in the density-matrix  $\delta \rho$  and deriving closed equations for  $\delta \rho_{\rm CC}$  which is able to determine the properties of the center region.

It suffices to illustrate the reduction of the degrees of freedom in the left bath. A direct computation yields

$$i \frac{\mathrm{d}}{\mathrm{d}t} \delta \rho_{\mathrm{LL}}(t) = [H_{\mathrm{LL}}(t), \delta \rho_{\mathrm{LL}}(t)] + F_{\mathrm{L}}(t) \tag{11}$$

where  $H_{\rm LL}(t) = H_{\rm LL}(0) + \delta H_{\rm LL}(t)$  and  $\delta H_{\rm LL}(t)$  is the external potential imposed on the left lead.  $F_L(t)$  represents the influence from the interior and can be extracted from (eq 8),

$$F_{\rm L}(t) = H_{\rm LC} \delta \rho_{\rm CL}(t) - \delta \rho_{\rm LC}(t) H_{\rm CL} + \Theta_{\rm LL}(t)$$
(12)

Now our key observation is that eqs 11 and 12 constitute an infinite-dimensional control problem with control variables  $\delta \rho_{\rm CL}$  and output  $\delta \rho_{\rm LL}$ . In practice, only the entries in  $\delta \rho_{\rm LL}$  near the interface (between  $\Omega_L$  and  $\Omega_C$ ) are needed. Such a largedimensional dynamical system with low-dimensional input and output can be effectively treated by using the reduced-order techniques. 41,42,63-65

2.2. General Petrov-Galerkin Projection Methods. Motivated by the development of reduced-order modeling techniques 63,64,66 that have been widely used in control problems, 43 circuit simulation, 42 and microelectromechanical systems, 65 etc., we propose a Petrov-Galerkin projection approach to derive a reduced model from the infinitedimensional LvN eq 11. The objective is to provide a reduced dynamics for the device region that captures both the transient and the steady state.

The first ingredient is to pick an appropriate subspace where the approximate solution is sought. To start with, we pick an *n*dimensional subspace  $\mathcal{V}_L$  spanned by a group of basis functions  $\{\varphi_i\}_{i=1}^{n_L}$ . The subspace can be expressed in a matrix form as  $V_{\rm L}$  =  $[\varphi_{\rm 1}, \varphi_{\rm 2}, ..., \varphi_{\rm n}]$ :  $\mathcal{V}_{\rm L}$  = range( $V_{\rm L}$ ). Throughout this paper, we will not distinguish a subspace  $\mathcal{V}_{L}$  and its matrix representation  $V_{L}$ .

As a simple illustration, the basis functions can be standard hat functions centered at certain grid points, as shown in Figure 2, which is popular in finite element discretizations. Alternatively Gaussian-like atomic orbitals can be used to form the subspace.

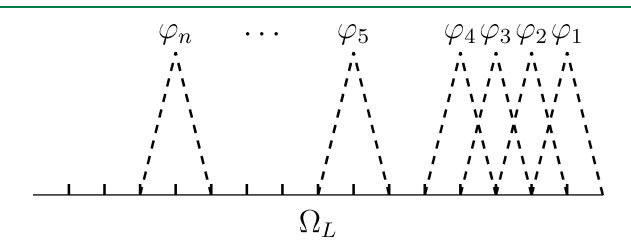


Figure 2. A diagram of hat functions on  $\Omega_L$  that span a subspace  $\mathcal{V}_L$  with dimension n.

In accordance with the Galerkin projection approach, one can seek a low-rank approximation of  $\delta \rho_{\rm LL}(t)$  as  $\delta \widetilde{\rho}_{\rm LL}$  in the following form,

$$\delta \widetilde{\rho}_{\rm LL}(t) := V_{\rm L} D_{\rm LL}(t) V_{\rm L}^* \tag{13}$$

Here  $D_{\rm LL}(t)$  is an  $n \times n$  matrix, whose entries are the coefficients of  $\delta \widetilde{\rho}_{\rm LL}(t)$  being expanded under the basis  $\{\varphi_i \varphi_j^*\}_{i,j=1}^n$ , and represents the nodal values of  $\delta \widetilde{\rho}_{\rm LL}(t)$  in the subspace spanned by  $V_{\rm L}$ . This representation automatically guarantees that the resulting density-matrix is Hermitian and semi positive-definite, as long as  $D_{\rm LL}$  has those properties. The residual error from this approximation can be directly deduced from the LvN eq 11 by subtraction,

$$\mathcal{E}(D_{\rm LL}, t) = iV_{\rm L} \frac{\rm d}{{\rm d}t} D_{\rm LL}(t) V_{\rm L}^* - [H(t), V_{\rm L} D_{\rm LL}(t) V_{\rm L}^*] - F_{\rm L}(t)$$
(14)

The second ingredient to determine  $D_{\rm LL}$  is by projecting the residual error to the orthogonal complement of a test subspace,  $W_{\rm L}$ , spanned by the columns of  $W_{\rm L}$ , that is

$$W_{\rm L}^* \mathcal{E}(D_{\rm LL}) W_{\rm L} = 0 \tag{15}$$

This yields a finite-dimensional system, and the reduction procedure described above is known in general as the Petrov-Galerkin projection, which has been a classical numerical method in the solutions of differential equations, <sup>67</sup> order-reduction problems, <sup>41,42</sup> and matrix equations. <sup>68,69</sup>

The reduced equation from the Petrov-Galerkin projection eqs 13 to 15 can be written as,

$$i \frac{\mathrm{d}}{\mathrm{d}t} D_{\mathrm{LL}}(t) = [\tilde{H}_{\mathrm{LL}} M_{\mathrm{L}}, D_{\mathrm{LL}}] - \tilde{F}_{\mathrm{L}}(t)$$
(16)

where the matrices are given by

$$M_{L} = (V_{L}^{*}W_{L})^{-1},$$

$$\tilde{H}_{LL}(t) = V_{L}^{*}H_{LL}(t)W_{L},$$

$$\tilde{F}_{L}(t) = M_{L}^{*}W_{L}^{*}F_{L}(t)W_{L}M_{L}$$
(17)

Notice that in eq 16 we have used the generalized notation of commutators. At this point, we will keep the subspaces

spanned by  $V_{\rm L}$  and  $W_{\rm L}$  at the abstract level, and the specific choices will be discussed in the next section.

The same model reduction procedure can be applied to the right lead and it yields a similar finite-dimensional equation,

$$i\frac{\mathrm{d}}{\mathrm{d}t}D_{\mathrm{RR}}(t) = [\tilde{H}_{\mathrm{RR}}M_{\mathrm{R}}, D_{\mathrm{RR}}] - \tilde{F}_{\mathrm{R}}(t) \tag{18}$$

Eqs 16 and 18 are related by the nonhomogeneous terms  $\tilde{F}_{\alpha}(t)$ ,  $\alpha=$  L, R that involve the evolution of  $\delta\rho_{C\alpha}$  and their Hermitian transpose.

In the center region, no reduction is needed and we will retain this part of eq 8. Therefore, we can construct a Petrov-Galerkin projection for the entire system, by gluing the subspaces as follows,

$$V = \begin{bmatrix} V_{\rm L} & 0 & 0 \\ 0 & I_{n_{\rm C}} & 0 \\ 0 & 0 & V_{\rm R} \end{bmatrix} \quad W = \begin{bmatrix} W_{\rm L} & 0 & 0 \\ 0 & I_{n_{\rm C}} & 0 \\ 0 & 0 & W_{\rm R} \end{bmatrix}$$
(19)

We seek an approximate solution

$$\delta\rho(t) \approx \delta\widetilde{\rho}(t) := VD(t)V^*$$
 (20)

for the projected dynamics of eq 6, such that,

$$W^*\mathcal{E}(D, t)W = 0 \tag{21}$$

where  $\mathcal{E}(D, t)$  is the residual error,

$$\mathcal{E}(D, t) = i \frac{\mathrm{d}}{\mathrm{d}t} \, \delta \widetilde{\rho}(t) - [H(t), \, \delta \widetilde{\rho}(t)] - \Theta(t) \tag{22}$$

Direct computations yield,

$$i\frac{\mathrm{d}}{\mathrm{d}t}D(t) = [H_{\mathrm{eff}}, D] + \widetilde{\Theta}(t)$$
 (23)

where  $H_{\text{eff}}$  is the reduced Hamiltonian,

$$H_{\text{eff}} = \begin{bmatrix} V_{\text{L}}^* H_{\text{LL}} W_{\text{L}} (V_{\text{L}}^* W_{\text{L}})^{-1} & V_{\text{L}}^* H_{\text{LC}} & 0 \\ H_{\text{CL}} W_{\text{L}} (V_{\text{L}}^* W_{\text{L}})^{-1} & H_{\text{CC}} & H_{\text{CR}} W_{\text{R}} (V_{\text{R}}^* W_{\text{R}})^{-1} \\ 0 & V_{\text{R}}^* H_{\text{RC}} & V_{\text{R}}^* H_{\text{RR}} W_{\text{R}} (V_{\text{R}}^* W_{\text{R}})^{-1} \end{bmatrix}$$
(24)

and  $\widetilde{\Theta}(t)$  is related to the nonhomogeneous term in (eq 7)

$$\widetilde{\Theta}(t) = M^* W^* \Theta(t) W M \tag{25}$$

Here the matrix M is block-diagonal,

$$M = \begin{bmatrix} (V_{\rm L}^* W_{\rm L})^{-1} & 0 & 0 \\ 0 & I_{n_{\rm C}} & 0 \\ 0 & 0 & (V_{\rm R}^* W_{\rm R})^{-1} \end{bmatrix}$$
(26)

It is worthwhile to point out that the subspaces can also be time-dependent. This offers the flexibility to pick subspaces that evolve in time. It should also be emphasized that our discussions regarding the Petrov-Galerkin projection are suitable for general cases and not limited to one-dimensional junction models, i.e., the typical lead-molecule-lead structures. With appropriate domain decomposition, it can be applied to high-dimensional systems with more general device structures.

**2.3. Selection of the Subspaces.** In this section, we discuss specific choices of the subspaces in the Galerkin-Petrov projection. Without loss of generality, we again start by

considering the left lead  $\Omega_L$ . Let  $\Omega_{\Gamma_L} \subset \Omega_L$  be a subdomain in the left lead that is adjacent to the center region, as shown in Figure 3. In our case, we pick  $\Omega_{\Gamma_L}$  in such a way that the

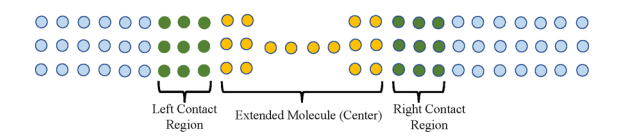


**Figure 3.** A schematic representation of junction model with contact regions in green.

remaining component in the lead has no coupling with the center region, i.e.,  $H_{i,j}=0$  for  $i\in\Omega_{\mathbb{C}}$  amd  $j\in\Omega_{\mathbb{L}}-\Omega_{\Gamma_{\!\!L}}$ . This imposes a lower bound on the size of the contact region. Similarly, for the right lead, we pick  $\Omega_{\Gamma_{\!\!R}}$  such that  $H_{i,j}=0$  for  $i\in\Omega_{\mathbb{C}}$  amd  $j\in\Omega_{\mathbb{R}}-\Omega_{\Gamma_{\!\!R}}$ .  $\Omega_{\Gamma_{\!\!L}}$  and  $\Omega_{\Gamma_{\!\!R}}$  are often referred to as contact regions that have direct coupling with the interior. <sup>54,70</sup>

In reduced-order modeling problems, the subspaces are often chosen based on how the input/control variables enter the large-dimensional system, e.g., see the review papers. <sup>41,42</sup> In our setting, we consider the dynamics in the left lead described by the density-matrix in the contact region. We pick the basis  $V_{\rm L}^*$  to act as a restriction operator from  $\Omega_{\rm L}$  to  $\Omega_{\rm L}$ ,

$$V_{\rm L}^* = [0, I_{n_{\rm F,L}}] \tag{27}$$

where  $I_{n_{\Gamma,\mathrm{L}}}$  is an identity matrix with the dimension  $n_{\Gamma,\mathrm{L}}$  being the number of grid points in  $\Omega_{\Gamma}$ .

The same procedure can be applied to the other lead region. When the subspaces are combined as in eq 19, we have

$$V = \begin{bmatrix} 0 & 0 & 0, \\ I_{n_{\Gamma,L}} & 0 & 0 \\ 0 & I_{n_{C}} & 0 \\ 0 & 0 & I_{n_{\Gamma,R}} \\ 0 & 0 & 0 \end{bmatrix}$$
 (28)

The entire density-matrix is approximated as in eq 20. It is now clear that V is a restriction operator to an extended center domain,  $\Omega_{\tilde{\mathbf{C}}} = \Omega_{\Gamma_{\!\! L}} \cup \Omega_{\mathbf{C}} \cup \Omega_{\Gamma_{\!\! R}}$ . Consequently, D in eq 23 becomes the density-matrix in  $\tilde{\mathbf{C}}$ ,

$$D(t) = \delta \widetilde{\rho}(t)|_{\Omega_{c} \times \Omega_{c}}$$
(29)

The subspaces  $W_{\rm L/R}$  remain to be chosen. Motivated by the Green's function approach for quantum transport,  $^{71-73}$  we consider the test space,

$$W_{\rm I}(\varepsilon) = (\varepsilon I - H_{\rm II})^{-1} V_{\rm I} \tag{30}$$

where  $\varepsilon \in \mathbb{C}$  is in the resolvent space of the Hamiltonian  $H_{\rm LL}$ . We require that  ${\rm Im}(\varepsilon) < 0$  to ensure the stability of the reduced models. In this case, it corresponds to the advanced Green's function as the imaginary part of  $\varepsilon$  goes to zero,

$$\lim_{\operatorname{Im}(\varepsilon) \to 0_{-}} W_{L}(\varepsilon) = G_{L}^{A}(\varepsilon) V_{L}$$
(31)

The selection of  $W_R$  is similar. Intuitively, the subspace W obtained this way represents the solution of the corresponding TDSE with initial conditions supported in the extended device

region  $\tilde{C}$ . We notice in passing that unlike the basis  $V_{\rm L}$  amd  $V_{\rm R}$ , the basis  $W_{\rm L}$  and  $W_{\rm R}$  do not have compact support.

We now examine the specific form of the reduced model (eq 23). With the specific choices of the subspaces as in eqs 27 and 30, one can simplify the matrix M in eq 26 as follows,

$$M_{\rm LL} = (V_{\rm L}^* W_{\rm L})^{-1} = \varepsilon I - H_{\Gamma_{\rm L}} \Gamma_{\rm L}(t) - \Sigma_{\rm L}(t, \varepsilon)$$
$$= : \varepsilon I - H_{\rm eff, L}(t, \varepsilon)$$
(32)

Similarly,

$$M_{\rm RR} = \varepsilon I - H_{\rm eff,R}(t,\,\varepsilon)$$
 (33)

Here  $\Sigma_{\alpha}$  is the self-energy<sup>24,74–76</sup> contributed by the left ( $\alpha$  = L) or right ( $\alpha$  = R) lead,

$$\Sigma_{\alpha}(t,\,\varepsilon) = H_{\Gamma_{\alpha},\alpha}(\varepsilon I - H_{\alpha,\alpha}(t))^{-1} H_{\alpha,\Gamma_{\alpha}} \tag{34}$$

and  $H_{\text{eff},\alpha}$  is the effective Hamiltonian associated with  $\Omega_{\Gamma_{\alpha}}^{77}$ 

$$H_{\text{eff},\alpha}(t,\,\varepsilon) = H_{\Gamma_{\alpha}\Gamma_{\alpha}}(t) + \Sigma_{\alpha}(t,\,\varepsilon)$$
 (35)

Overall, the effective Hamiltonian  $H_{
m eff}$  in eq 23 is simplified to

$$H_{\text{eff}}(t) := H_{C}(t) + \Sigma(t, \varepsilon)$$
 (36)

where  $H_{\rm C}$  is the Hamiltonian restricted in the extended center region  $\Omega_{\tilde{\rm C}}$ ,

$$H_{\mathcal{C}}(t) := H(t)|_{\Omega_{\tilde{c}} \times \Omega_{\tilde{c}}} \tag{37}$$

and  $\boldsymbol{\Sigma}$  is a block-wise diagonal matrix that incorporates the self-energies of two leads,

$$\Sigma(t,\,\varepsilon) = \begin{bmatrix} \Sigma_{\rm L}(t,\,\varepsilon) & 0 & 0 \\ 0 & 0 & 0 \\ 0 & 0 & \Sigma_{\rm R}(t,\,\varepsilon) \end{bmatrix} \tag{38}$$

The self-energy (eq 34) involves the inverse of a large-dimensional (or infinite-dimensional) matrix. Similar to the inversion in eq 4, it can be efficiently computed using a recursive algorithm, which has been well-documented. 54,78,79 The self-energy only needs to be computed once for constant external potential, and for periodic external potentials, it can be precomputed for one period.

Let  $\rho_{\rm C}$  be the density-matrix restricted in the extended center region  $\Omega_{\bar{\rm C}}$ , i.e.,

$$\rho_{\mathcal{C}}(t) := \rho(t)|_{\Omega_{\mathcal{C}} \times \Omega_{\mathcal{C}}} = D(t) + \rho_{\mathcal{C}}(0)$$
(39)

The reduced model for this part of the density-matrix can now be written as,

$$i \frac{\mathrm{d}}{\mathrm{d}t} \rho_{\mathrm{C}}(t) = [H_{\mathrm{eff}}(t), \rho_{\mathrm{C}}(t)] + \Theta_{\mathrm{C}}(t)$$
(40)

With our choice of the subspaces, the reduced dynamics is driven by the effective Hamiltonian  $H_{\rm eff}$ . The nonhomogeneous term  $\Theta_{\rm C}$  embodies the effect of the potential,

$$\Theta_{\mathcal{C}}(t) = M^* \tilde{V}^* (\varepsilon^* I - H)^{-1} [H, \overline{\rho}_0] (\varepsilon I - H)^{-1} \tilde{V} M$$
(41)

where  $\overline{\rho}_0 = \rho_0 - VV^*\rho_0 VV^*$ , M is computed from eq 32 and  $\tilde{V}$  is in the form of

$$\tilde{V} = \begin{pmatrix} V_{L} & -H_{LC} & 0 \\ -H_{C\Gamma_{L}}V_{L}^{*}(\varepsilon - H_{LL})V_{L} & \varepsilon - H_{CC} & -H_{C\Gamma_{R}}V_{R}^{*}(\varepsilon - H_{RR})V_{R} \\ 0 & -H_{RC} & V_{R} \end{pmatrix}$$
(42)

The practical implementation of the reduced model hinges on the availability of efficient algorithms to compute (i) the self-energy (34); (ii) the initial density-matrix in the center and contact region; and (iii) the nonhomogeneous term (eq 41). The computation of the self-energy and the initial densitymatrix, as previously discussed, can be computed using the selective inversion techniques, which is applicable for problems that can be cast into the form of (eq 4) where the Green's function is accompanied by sparse vectors. As for the nonhomogenous term, we find that  $V_{\alpha}$  and  $H_{\alpha,C}$ ,  $\alpha = L$ , R have nonzero elements only associated with those degrees of freedom in the domain  $\Omega$ , which implies the sparsity of  $\tilde{V}$ . Upon closer inspection, we find that the product of inverse matrices in  $\Theta(t)$ , i.e.,  $(\varepsilon^*I - H)^{-1}\Theta(t)(\varepsilon I - H)^{-1}$ , can be written as a sum of single matrix inverses (partial fractions), provided that  $\varepsilon$  is in the resolvent of H and  $\text{Im}(\varepsilon) \neq 0$ . For example, we have,

$$(zI - H)^{-1}(\varepsilon I - H)^{-1} = \frac{1}{\varepsilon - z}((zI - H)^{-1} - (\varepsilon I - H)^{-1})$$

Consequently, all those blocks can be written in the general form (eq 4), and one compute  $\Theta_C$  efficiently by using the selective inversion techniques.<sup>53</sup>

**2.4.** Properties of the Reduced Models. 2.4.1. Hermitian Property of  $\rho_C(t)$ . The projection method produces an approximation of the density-matrix in the extended center region, leading to an open quantum-mechanical model that can be subsequently used to predict the current. The influence from the infinite leads, through the self-energy, has been implicitly incorporated into the effective Hamiltonian. By taking the Hermitian of the reduced model (eq 40), and noticing the anti-Hermitian property of the term  $\widetilde{\Theta}$ , we find that  $\rho_C^*$  also satisfies (eq 40) with initial condition  $\rho_C^*(0)$ . As  $\rho_C(0)$  is Hermitian, and in light of the uniqueness of the solution, we obtain the Hermitian property for  $\rho_C(t)$ .

2.4.2. Stability of the Reduced Models. Next, let us turn to the analysis of stability. Since the stability of the linear nonhomogeneous system is implied by the stability of the homogeneous system, we focus on the homogeneous case in eq 40 to study its stability. The problem can be addressed as the stability of a finite system X(t),

$$i \frac{\mathrm{d}}{\mathrm{d}t} X(t) = H_{\mathrm{eff}}^*(t)X(t) - X(t)H_{\mathrm{eff}}(t),$$

$$X(0) = \rho_{\mathrm{C}}(0) \tag{43}$$

where  $H_{\text{eff}} = H_{\text{C}} + \Sigma$ . Since  $\rho_{\text{C}}(0)$  has an eigen-decomposition  $\rho_{\text{C}}(0) = \sum_{l} n_{l} \psi_{l}^{0} \psi_{l}^{0*}$ , it is not difficult to verify that  $X(t) = \sum_{l} n_{l} \psi_{l}(t) \psi_{l}^{*}(t)$  is the solution of eq 43 if  $\psi_{l}(t)$  satisfies

$$i \frac{\mathrm{d}}{\mathrm{d}t} \psi_l(t) = H_{\text{eff}}^*(t) \psi_l(t),$$
  
$$\psi_l(0) = \psi_l^0$$
 (44)

It suffices to analyze the stability of eq 44.

There exists a decomposition  $H^*_{\rm eff}(t) = A_1(t) + iA_2(t)$ , where  $A_1$  and  $A_2$  are real-valued symmetric matrices and  $A_2$  is determined from  $\Sigma$  due to the Hermitian property of  $H_{\rm C}$ . Further computation yields,

$$A_2(t) = \begin{pmatrix} \widetilde{\Phi}_L \Lambda_L(t) \widetilde{\Phi}_L^* & 0 & 0 \\ 0 & 0 & 0 \\ 0 & 0 & \widetilde{\Phi}_R \Lambda_R(t) \widetilde{\Phi}_R^* \end{pmatrix}$$

$$\tag{45}$$

$$\lambda_I^{\alpha} = \operatorname{Im} \left( \frac{1}{\varepsilon^* - \mu_I^{\alpha}} \right) \tag{46}$$

where  $\mu_I^{\alpha}$  is the eigenvalue of  $H_{\alpha,\alpha}$ .

To ensure the stability, it is enough to require that  $A_2$  has only nonpositive eigenvalues, <sup>80</sup> i.e.,

$$\lambda_l^{\alpha} = \operatorname{Im}\left(\frac{1}{\varepsilon^* - \mu_l^{\alpha}}\right) = \frac{\operatorname{Im}(\varepsilon)}{|\varepsilon^* - \mu_l^{\alpha}|^2} \le 0 \tag{47}$$

This confirms that when  $\varepsilon$  has a negative imaginary part, the stability of eq 40 is guaranteed.

**2.5.** Higher Order Subspace Projections. The Galerkin-Petrov projection method can be extended to higher order, by expanding the subspaces  $V_{\rm L/R}$  and  $W_{\rm L/R}$  to higher dimensions. Here we provide two options to extend the current subspaces.

2.5.1. Expanding the Contact Region. One straightforward approach is to keep the choices of V and W according to eq 27 and eq 30 but increase the size of the region  $\Omega_{\Gamma}$  to increase the subspace. Through numerical tests, we observe that this is a rather simple alternative, and it captures steady state current with subspaces of relatively small dimensions  $n_{\Gamma}$ .

2.5.2. Block Krylov Subspaces. Another approach, as motivated by the block Krylov techniques<sup>81</sup> for large-dimensional dynamical systems, is to expand the subspace  $V_{\rm L}$  to the block Krylov subspace,

$$V_{L,m} = [V_L H_{LL} V_L \cdots H_{LL}^{m-1} V_L] = : \mathcal{K}_m(H_{LL}; V_L)$$
(48)

The corresponding  $W_{1,m}$  has a similar structure,

$$W_{L,m} = [W_L V_L \cdots H_{LL}^{m-2} V_L] = : \mathcal{K}_m(H_{LL}; W_L)$$
(49)

The Krylov subspaces are composed of a generating matrix and a starting block. In order to keep the additional blocks full rank, we pick  $V_{\rm L}$  based on the interaction range in  $H_{\rm LL}$ . For example, if  $H_{\rm LL}$  is based on a one-dimensional nearest-neighbor Hamiltonian, then we pick  $n_{\Gamma}=1$  to define  $V_{\rm L}$ , which would be a one-dimensional vector; we picked  $n_{\Gamma}=2$  for a next nearest neighbor Hamiltonian, etc.

### 3. NUMERICAL EXPERIMENTS AND DISCUSSIONS

To test the reduction method, we consider a one-dimensional two-lead molecular junction model within a TB setting, similar to the setup in Zelovich et al. More specifically, in the computation, the leads are represented by two finite atomic chains with increasing lengths ( $n_L$  and  $n_R$ , respectively) to mimic an infinite dimensional system and eliminate the finite

size effect. The extended molecule with length  $n_{\rm C}$  is represented by a finite atomic chain coupled with both leads. Here, the atomic unit is used throughout the paper if not stated otherwise.

Initially, the system is configured in thermodynamic equilibrium at temperature T=0 K, with all single-particle levels occupied up to the Fermi energy  $\varepsilon_{\rm F}=0.3$  a.u. The onsite energy is taken as  $\alpha=1$  au, and the hopping integral between nearest neighbors is  $\beta=-0.5$  au. At time  $t=0_+$ , a bias potential is switched on in the electrodes. With the computed density-matrix, we study the bond current through the molecular junction to monitor the dynamics, using the formula  $^{38}$ 

$$I(t) = 2\beta \operatorname{Im}[\rho_{i,i+1}(t)] \tag{50}$$

For the time propagation of the density-matrix, we use the fourth-order Runge–Kutta scheme to solve the full model (eq 2), as well as (eq 40). We fix the size of the center region  $n_{\rm C}$  = 20 and simulate the system under two different types of external potentials: (1) constant biased potential:  $U_{\rm L/R} = \mp \frac{\delta U}{2}$  to mimic direct current (DC) circuit and (2) time-dependent potential: a sinusoidal signal in the left lead,  $U_{\rm L} = \delta U \sin \omega t$ , to mimic an alternating current (AC) and the potential on the right stays at zero.

In principle, the bath size needs to be infinite to model the two semi-infinite leads; but in practical computations, one can only treat a system of finite-size and expect the system to reach a steady state in the limit as the bath size goes to infinity. We pick this microcanonical formulation as our starting full model, which can be viewed as two sufficiently large (but finite) charged electrodes that discharge across a molecular junction. The electric current through the conjunction can be calculated without implementing scattering boundary conditions and by the use of effective one-electron time-dependent LvN equations. An alternative choice is the driven LvN method presented in ref 40 where a target density is supplied to act like the source injecting electrons from electrodes. When the driving rate is zero, this model coincides with the microcanonical setup.

Numerically, we examine such size effect by varying  $n_{\rm L}/n_{\rm R}$ and observing the current in the center region. More specifically, we run direct simulations of eq 2 using  $n_L = n_R$ = 200, 500, 1000, 2000. Our results (Figures 4 and 5) suggest that, for the constant potential case, the electric current gradually develops into a steady state until the propagating electronic waves reach the ends of the leads and get reflected toward the bridge. As we extend the leads size to  $n_I = n_R =$ 1000, the backscattering effect occurs much later and is no longer observed within the time window of our simulation. For the dynamic potential case, we observe periodic changes of the electric current. Size effects become insignificant when the size is increased to  $n_L = n_R = 500$  over the duration of the simulation. We also examine the occupancy of two leads at steady-state (double occupancy of each orbital assumed). When  $n_L = n_R = 500$ , the occupations are close to the Fermi distributions at zero temperature. We point out that this effort of using a sufficiently large bath size is only to generate a faithful result from the full model (eq 2), which will be used as a reference to examine the accuracy of the reduced model (eq 40). These degrees of freedom will not be explicitly resolved in the reduced model.

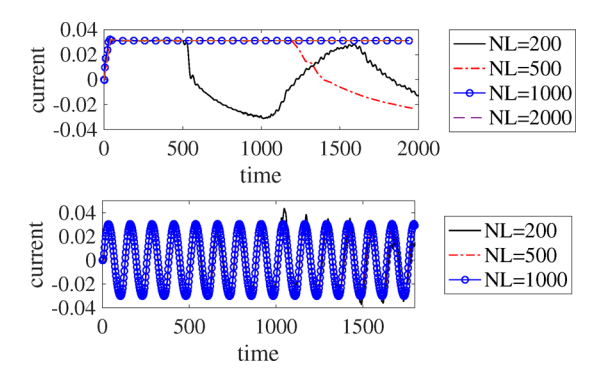


**Figure 4.** The finite size effect on the electric current. The figures show the time evolution of the currents through a junction coupled with two finite leads of varying sizes  $n_{\rm L}=n_{\rm R}$ . The number of atoms in the extended molecule (center region) remains the same,  $n_{\rm C}=20$ . Top: constant bias potential  $U_{\rm L}=-U_{\rm R}=0.1$  a.u. Bottom: dynamic potential  $U_{\rm L}=0.2\,\sin(0.05t)$  a.u.,  $U_{\rm R}=0$ .

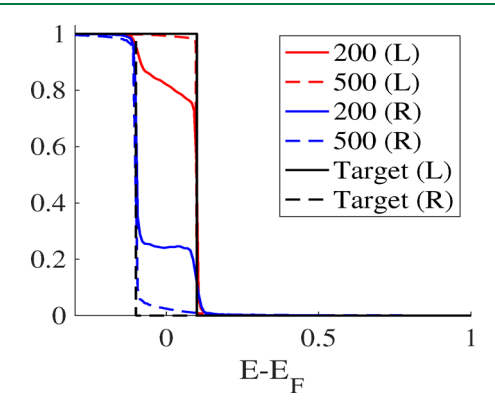


**Figure 5.** Steady-state occupations obtained using lead models of  $n_{\rm L} = n_{\rm R} = 200$  (solid line) and  $n_{\rm L} = n_{\rm R} = 500$  (dashed line) compared to the corresponding target lead-equilibrium step-function distributions (black), with the other same conditions in Figure 4.

Next we compute the transient current of the DC circuit (case 1) from the effective reduced models (eq 40) and compare it with the current from the full model (eq 2) to evaluate the accuracy of the reduction method. Again, the results from the full model are generated with a sufficiently large bath. We examine the different choices of increasing the subspaces (as discussed in section 2.5). In particular, in Figure 6 we show the numerical results from using the subspaces (eq 27) and (eq 30), and we choose the dimension  $n_{\Gamma}$  from 1 to 10. First we notice that no recurrent phenomenon is observed, which can be attributed to the nonhomogeneous term  $\Theta_C(t)$  as well as the self-energy in eq 40, since they take into account the influence from the bath. The results improve as we expand the subspace,  $V_{\alpha}$  and  $W_{\alpha}$ ,  $\alpha = L/R$  in eq 19. The steady state current has already been well captured by the reduced model with dimensions  $n_{\Gamma} = 2$ , while the transient results improve as we expand  $n_{\Gamma}$ , and we arrive at a very satisfactory result when  $n_{\Gamma}=4.$ 

We also examine, as shown in Figure 6, the occupation of the energy states in order to make sure our current method still follows Pauli's exclusion principle as well as the positivity of the density matrix. We observe that the occupations remain from 0 to 1 throughout the simulations (double occupancy of each orbital assumed), and after t = 50 au, the system arrives at steady-states and the occupations start to settle.

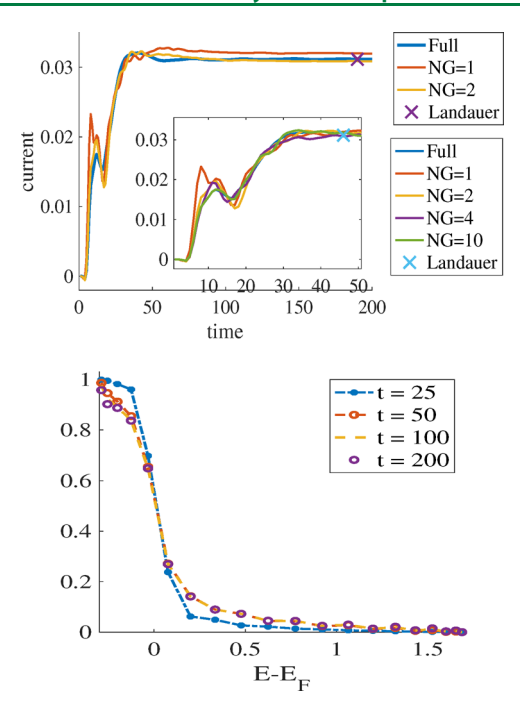


**Figure 6.** The simulation of the DC circuit (constant bias  $U_L = -U_R = 0.1$  au). The full system is modeled with a sufficiently large bath  $n_L = n_R = 500$ ,  $n_C = 20$ . The shift parameter is set to  $\varepsilon = 0.3-0.1i$ . The left panel shows the time history of the current from the reduced model (eq 40) with different subspace dimensions  $n_\Gamma$ , compared to the result from the full model (eq 2). The subspaces are chosen from (eq 27) and (eq 30) by extending the contact region  $\Omega_\Gamma$ . The inset shows the zoomed-up view of the transient stage of the current. The right panel shows the occupations of the center region at different time shots with the subspace dimensions  $n_\Gamma = 1$ .

It is worthwhile to comment on the dimension of the reduced model. The density-matrix in the full model has dimension  $(n_{\rm C} + n_{\rm L} + n_{\rm R})^2$  In contrast, the dimension of the reduced density-matrix is  $(n_{\rm C} + 2n_{\rm \Gamma})^2$ , which offers drastic reduction in terms of the number of degrees of freedom.

We now test the Krylov subspaces according to (eq 48) and (eq 49), as shown in Figure 7. The subspaces can be expanded by increasing m. The steady state is well captured when m = 2, while the transient requires higher-order approximations. Our

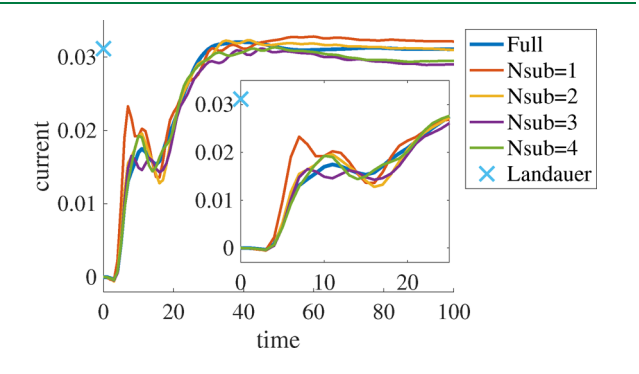


**Figure 7.** The results from the simulation of the DC circuit (constant bias  $U_{\rm L}=-U_{\rm R}=0.1$  au). The figure shows the time evolution of the current from the reduced model (eq 40), generated by the block Krylov subspaces (eq 48 and eq 49) for various choices of dimensions (Nsub = m), with parameter  $\varepsilon=0.3-0.01i$ . The results are compared to the result from the full model (eq 2). The inset shows the transient stage of the current.

observation is that in order to achieve the same accuracy, we need larger subspaces than the previous approach. On the other hand, the Krylov subspace approach is more robust in the regime where  $\mathrm{Im}(\varepsilon)$  is close to zero.

Another important factor that plays a role in the reduced model is the selection of the parameter  $\varepsilon$ , which can be viewed as an interpolation point for the self-energy. Therefore, we study the dependence of  $\varepsilon$  in the reduced models, by observing the electric current at steady state for various different choices of  $\varepsilon$ . For the imaginary part, we require  $\mathrm{Im}(\varepsilon)$  to be strictly less than zero to ensure that the self-energy (eq 34) is well-defined and (eq 40) has the stability assurance. We start with  $\mathrm{Im}(\varepsilon) = -0.15$ . When  $\mathrm{IIm}(\varepsilon)$  is further decreased (<0.01), the electric current exhibits oscillations around the true value of the steady state. For the real part of  $\varepsilon$ , the optimal value appears around the Fermi energy. See Figure 8. This suggests that  $\varepsilon$  should be around the Fermi level with a small imaginary part, although when the imaginary part is too small, the numerical robustness might be affected.

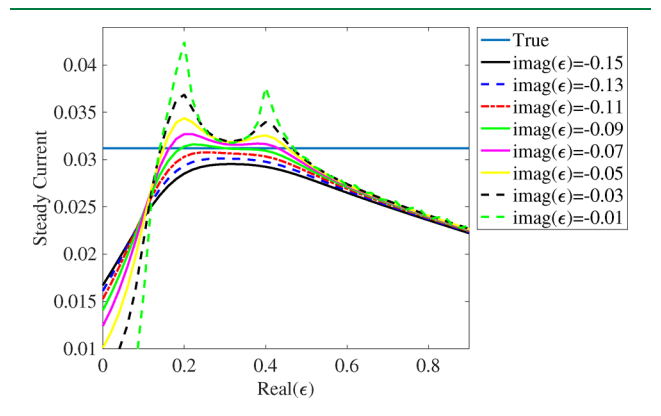


**Figure 8.** The example of DC circuit with constant bias  $(U_L = -U_R = 0.1 \text{ a.u.})$ . The Figure shows the steady-state current predicted by the reduced model (eq 40) using various choices of the parameter  $\varepsilon$  with  $n_\Gamma = 1$ .

Finally, we turn to the example of the AC circuit. Since a time-dependent external potential is imposed,  $H_{\rm C}$  and  $\Theta_{\rm C}$  in eq 40 are time-dependent as well. They need to be evaluated at each time step. Due to the periodic property, it suffices to precompute  $H_{\rm C}(t)$  and  $\Theta_{\rm C}(t)$  within one time period. As shown in Figure 9, a periodic electric current has been reproduced by the reduced model (eq 40), and the accuracy also improves as we expand the subspace size  $n_{\rm F}$ . The electric current is already well captured when  $n_{\rm F}=4$ .

### 4. SUMMARY

We have proposed to formulate the quantum transport problem in a molecular junction coupled with infinite baths as a reduced-order modeling problem. The goal is to derive a finite quantum system with open boundary conditions. Motivated by the works in refs 36, 38, and 39, we work with the density-matrix and obtain reduced Liouville-von Neumann equations for the center and contact regions. The reduced equations are derived using a systematic projection formalism, together with appropriate choices of the subspaces. Numerical experiments have shown that the reduced model is very effective in capturing the steady-state electric current as well as the transient process of the electric current. The accuracy increases as we expand the contact regions in the reduced

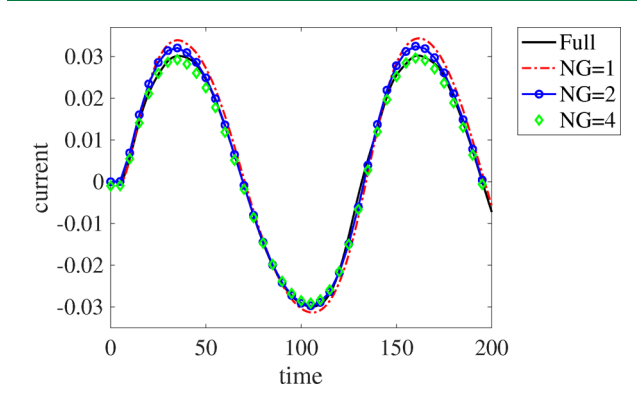


**Figure 9.** The example of an AC circuit with time-dependent potential  $U_{\rm L}(t)=0.2\,\sin(0.05t)$  a.u.,  $U_{\rm R}=0$ . This figure displays the time evolution of the currents from the reduced models with different subspace dimensions  $n_{\rm L}$ , compared to that from the full model. The parameter  $\varepsilon=0.3-0.1i$  is used.

model. The reduced model has been very effective in preventing the backscattering at the boundary. The fact that the effective Hamiltonian contains an imaginary part, and the fact that the self-energy is concentrated at the boundary, indicate a strong connection to the complex absorbing potential (CAP) method. However, the effective Hamiltonian is derived from a reduced-order method, which takes into account the electron structure in the bath, rather than empirically constructed. On the other hand, the projection to higher-order Krylov subspaces leads to models that go beyond the CAP method.

In order to demonstrate the reduction procedure, we have considered a one-dimensional junction system. The validity of the projection approach is not restricted to the one-dimensional system. It can be applied to general coupled system-bath dynamics that require model reduction due to the computational complexity. The extension to systems that are of direct practical interest is underway. Another possible extension is the data-driven implementation of reduced-order modeling. In this case, rather than computing the matrices in the reduced models from the underlying quantum mechanical models, they are inferred from observations. <sup>81,83</sup>

Self-consistency has not been included in the Liouville-von Neumann equation, especially the Coulomb potential, which in the linear response regime, leads to a dense matrix<sup>84</sup> from the Hartree term. This creates considerable difficulty for the reduce-order modeling since the partition (eq 24) is no longer reasonable. However, the Coulomb and exchange correlation are known to be important for the Coulomb blockade phenomena.<sup>85</sup> This difficulty in the modeling of quantum transport has also been pointed out in refs 27 and 86. In practice, this is often dealt with by solving Poisson's equation in a relatively larger domain with Dirichlet boundary conditions.<sup>23</sup> We will address this issue under the framework of reduced-order modeling in separate works.

## **■** AUTHOR INFORMATION

### **Corresponding Authors**

Weiqi Chu — Department of Mathematics, University of California, Los Angeles, Los Angeles, CA 90095, United States; Department of Mathematics, Pennsylvania State University, University Park, PA 16802, United States; <sup>⑤</sup> orcid.org/0000-0002-1476-2925; Email: chu@math.ucla.edu

I

Xiantao Li — Department of Mathematics, Pennsylvania State University, University Park, PA 16802, United States; Email: xli@math.psu.edu

Complete contact information is available at: https://pubs.acs.org/10.1021/acs.jctc.9b01090

#### Notes

The authors declare no competing financial interest.

### ACKNOWLEDGMENTS

This research was supported by NSF under grants DMS-1619661 and DMS-1819011.

### REFERENCES

- (1) Aviram, A. Molecular electronics-science and technology. *Angew. Chem.* **1989**, *101*, 536–537.
- (2) Reed, M. A. Molecular-scale electronics. Proc. IEEE 1999, 87, 652-658
- (3) Joachim, C.; Gimzewski, J. K.; Aviram, A. Electronics using hybrid-molecular and mono-molecular devices. *Nature* **2000**, *408*, 541.
- (4) Aradhya, S. V.; Venkataraman, L. Single-molecule junctions beyond electronic transport. *Nat. Nanotechnol.* **2013**, *8*, 399.
- (5) Cahen, D.; Kahn, A.; Umbach, E. Energetics of molecular interfaces. *Mater. Today* **2005**, *8*, 32–41.
- (6) Cahen, D.; Kahn, A. Electron energetics at surfaces and interfaces: Concepts and experiments. *Adv. Mater.* **2003**, *15*, 271–277.
- (7) Hwang, J.; Wan, A.; Kahn, A. Energetics of metal-organic interfaces: New experiments and assessment of the field. *Mater. Sci. Eng., R* **2009**, *64*, 1–31.
- (8) Brabec, C. J. Organic photovoltaics: Technology and market. *Sol. Energy Mater. Sol. Cells* **2004**, *83*, 273–292.
- (9) Brédas, J.-L.; Norton, J. E.; Cornil, J.; Coropceanu, V. Molecular understanding of organic solar cells: The challenges. *Acc. Chem. Res.* **2009**, *42*, 1691–1699.
- (10) Poulsen, J. A.; Rossky, P. J. Path integral centroid molecular-dynamics evaluation of vibrational energy relaxation in condensed phase. *J. Chem. Phys.* **2001**, *115*, 8024–8031.
- (11) Potter, S.; Skinner, M. J. On transport integration: A contribution to better understanding. *Futures* **2000**, *32*, 275–287.
- (12) Everitt, K.; Egorov, S.; Skinner, J. Vibrational energy relaxation in liquid oxygen. *Chem. Phys.* **1998**, 235, 115–122.
- (13) Nibbering, E. T.; Wiersma, D. A.; Duppen, K. Femtosecond non-Markovian optical dynamics in solution. *Phys. Rev. Lett.* **1991**, *66*, 2464
- (14) Pshenichnikov, M. S.; Duppen, K.; Wiersma, D. A. Timeresolved femtosecond photon echo probes bimodal solvent dynamics. *Phys. Rev. Lett.* **1995**, *74*, 674.
- (15) Joo, T.; Jia, Y.; Fleming, G. R. Ultrafast liquid dynamics studied by third and fifth order three pulse photon echoes. *J. Chem. Phys.* 1995, 102, 4063–4068.
- (16) Becker, P. C.; Fragnito, H. L.; Bigot, J. Y.; Brito Cruz, C. H.; Fork, R. L.; Shank, C. V. Femtosecond photon echoes from molecules in solution. *Phys. Rev. Lett.* **1989**, *63*, 505.
- (17) Lang, M.; Jordanides, X.; Song, X.; Fleming, G. Aqueous solvation dynamics studied by photon echo spectroscopy. *J. Chem. Phys.* **1999**, *110*, 5884–5892.
- (18) Landauer, R. Electrical resistance of disordered one-dimensional lattices. *Philos. Mag.* **1970**, *21*, 863–867.
- (19) Büttiker, M.; Imry, Y.; Landauer, R.; Pinhas, S. Generalized many-channel conductance formula with application to small rings. *Phys. Rev. B: Condens. Matter Mater. Phys.* **1985**, 31, 6207.
- (20) Büttiker, M. Four-terminal phase-coherent conductance. *Phys. Rev. Lett.* **1986**, *57*, 1761.

- (21) Cini, M. Time-dependent approach to electron transport through junctions: General theory and simple applications. *Phys. Rev. B: Condens. Matter Mater. Phys.* **1980**, 22, 5887.
- (22) Lang, N. Resistance of atomic wires. Phys. Rev. B: Condens. Matter Mater. Phys. 1995, 52, 5335.
- (23) Taylor, J.; Guo, H.; Wang, J. Ab initio modeling of quantum transport properties of molecular electronic devices. *Phys. Rev. B: Condens. Matter Mater. Phys.* **2001**, *63*, 245407.
- (24) Brandbyge, M.; Mozos, J.-L.; Ordejón, P.; Taylor, J.; Stokbro, K. Density-functional method for nonequilibrium electron transport. *Phys. Rev. B: Condens. Matter Mater. Phys.* **2002**, *65*, 165401.
- (25) Hohenberg, P.; Kohn, W. Inhomogeneous electron gas. Phys. Rev. 1964, 136, B864.
- (26) Kohn, W.; Sham, L. J. Self-consistent equations including exchange and correlation effects. *Phys. Rev.* **1965**, *140*, A1133–A1138.
- (27) Kurth, S.; Stefanucci, G.; Almbladh, C.-O.; Rubio, A.; Gross, E. K. Time-dependent quantum transport: A practical scheme using density functional theory. *Phys. Rev. B: Condens. Matter Mater. Phys.* **2005**, 72, 035308.
- (28) Runge, E.; Gross, E. K. Density-functional theory for time-dependent systems. *Phys. Rev. Lett.* **1984**, *52*, 997.
- (29) Stefanucci, G.; Almbladh, C.-O. Time-dependent quantum transport: An exact formulation based on TDDFT. EPL 2004, 67, 14.
- (30) Burke, K.; Car, R.; Gebauer, R. Density functional theory of the electrical conductivity of molecular devices. *Phys. Rev. Lett.* **2005**, *94*, 146803.
- (31) Cheng, C.-L.; Evans, J. S.; Van Voorhis, T. Simulating molecular conductance using real-time density functional theory. *Phys. Rev. B: Condens. Matter Mater. Phys.* **2006**, 74, 155112.
- (32) Stefanucci, G.; Almbladh, C.-O. Time-dependent partition-free approach in resonant tunneling systems. *Phys. Rev. B: Condens. Matter Mater. Phys.* **2004**, *69*, 195318.
- (33) Baer, R.; Seideman, T.; Ilani, S.; Neuhauser, D. Ab initio study of the alternating current impedance of a molecular junction. *J. Chem. Phys.* **2004**, *120*, 3387–3396.
- (34) Varga, K. Time-dependent density functional study of transport in molecular junctions. *Phys. Rev. B: Condens. Matter Mater. Phys.* **2011**, 83, 195130.
- (35) Antoine, X.; Besse, C. Unconditionally stable discretization schemes of non-reflecting boundary conditions for the one-dimensional Schrödinger equation. *J. Comput. Phys.* **2003**, *188*, 157–175.
- (36) Sánchez, C. G.; Stamenova, M.; Sanvito, S.; Bowler, D.; Horsfield, A. P.; Todorov, T. N. Molecular conduction: Do time-dependent simulations tell you more than the Landauer approach? *J. Chem. Phys.* **2006**, *124*, 214708.
- (37) Subotnik, J. E.; Hansen, T.; Ratner, M. A.; Nitzan, A. Nonequilibrium steady state transport via the reduced density matrix operator. *J. Chem. Phys.* **2009**, *130*, 144105.
- (38) Zelovich, T.; Kronik, L.; Hod, O. State representation approach for atomistic time-dependent transport calculations in molecular junctions. *J. Chem. Theory Comput.* **2014**, *10*, 2927–2941.
- (39) Zelovich, T.; Kronik, L.; Hod, O. Molecule-Lead coupling at molecular junctions: Relation between the real- and state-space perspectives. *J. Chem. Theory Comput.* **2015**, *11*, 4861–4869.
- (40) Zelovich, T.; Hansen, T.; Liu, Z.-F.; Neaton, J. B.; Kronik, L.; Hod, O. Parameter-free driven Liouville-von Neumann approach for time-dependent electronic transport simulations in open quantum systems. *J. Chem. Phys.* **2017**, *146*, 092331.
- (41) Bai, Z. Krylov subspace techniques for reduced-order modeling of large-scale dynamical systems. *Appl. Numer. Math.* **2002**, *43*, 9–44.
- (42) Freund, R. W. Krylov-subspace methods for reduced-order modeling in circuit simulation. *J. Comput. Appl. Math.* **2000**, *123*, 395–421.
- (43) Villemagne, C. d.; Skelton, R. E. Model reductions using a projection formulation. *Int. J. Control* **1987**, *46*, 2141–2169.
- (44) Smith, G. D.; Smith, G. D. Numerical solution of partial differential equations: Finite difference methods; Oxford University Press, 1985.

- (45) Johnson, C. Numerical solution of partial differential equations by the finite element method; Courier Corporation, 2012.
- (46) Lambert, J. D.; Lambert, J. Computational methods in ordinary differential equations; Wiley: London, 1973; Vol. 23.
- (47) Morton, K. W.; Mayers, D. F. Numerical solution of partial differential equations: An introduction; Cambridge University Press, 2005.
- (48) Beck, T. L. Real-space mesh techniques in density-functional theory. *Rev. Mod. Phys.* **2000**, 72, 1041.
- (49) Zelovich, T.; Kronik, L.; Hod, O. Driven Liouville von Neumann approach for time-dependent electronic transport calculations in a nonorthogonal basis-set representation. *J. Phys. Chem. C* **2016**, *120*, 15052–15062.
- (50) Sankey, O. F.; Niklewski, D. J. Ab initio multicenter tight-binding model for molecular-dynamics simulations and other applications in covalent systems. *Phys. Rev. B: Condens. Matter Mater. Phys.* **1989**, *40*, 3979.
- (51) Inglesfield, J. E. A method of embedding. J. Phys. C: Solid State Phys. 1981, 14, 3795.
- (52) Kelly, P. J.; Car, R. Green's-matrix calculation of total energies of point defects in silicon. *Phys. Rev. B: Condens. Matter Mater. Phys.* **1992**, *45*, 6543.
- (53) Lin, L.; Yang, C.; Meza, J. C.; Lu, J.; Ying, L.; E, W. SelInv—An algorithm for selected inversion of a sparse symmetric matrix. *ACM Trans. Math. Softw.* **2011**, *37*, 1.
- (54) Williams, A.; Feibelman, P. J.; Lang, N. Green's-function methods for electronic-structure calculations. *Phys. Rev. B: Condens. Matter Mater. Phys.* **1982**, *26*, 5433.
- (55) Godfrin, E. M. A method to compute the inverse of an n-block tridiagonal quasi-Hermitian matrix. *J. Phys.: Condens. Matter* **1991**, *3*, 7843.
- (56) Pecchia, A.; Penazzi, G.; Salvucci, L.; Di Carlo, A. Non-equilibrium Green's functions in density functional tight binding: Method and applications. *New J. Phys.* **2008**, *10*, 065022.
- (57) Li, X. An atomistic-based boundary element method for the reduction of molecular statics models. *Comput. Method Appl. M.* **2012**, 225–228, 1–13.
- (58) Li, X.; Lin, L.; Lu, J. PEXSI-Σ: A Green's function embedding method for Kohn-Sham density functional theory. *Ann. Math. Sci. Appl.* **2018**, *3*, 441–472.
- (59) Gross, E.; Kohn, W. Local density-functional theory of frequency-dependent linear response. *Phys. Rev. Lett.* **1985**, *55*, 2850.
- (60) Dobson, J. F.; Bünner, M.; Gross, E. Time-dependent density functional theory beyond linear response: An exchange-correlation potential with memory. *Phys. Rev. Lett.* **1997**, *79*, 1905.
- (61) Gunnarsson, O.; Lundqvist, B. I. Exchange and correlation in atoms, molecules, and solids by the spin-density-functional formalism. *Phys. Rev. B* **1976**, *13*, 4274.
- (62) Li, X. Absorbing boundary conditions for time-dependent Schrödinger equations: A density-matrix formulation. *J. Chem. Phys.* **2019**, *150*, 114111.
- (63) Gugercin, S.; Stykel, T.; Wyatt, S. Model reduction of descriptor systems by interpolatory projection methods. *SIAM J. Sci. Comput.* **2013**, *35*, B1010–B1033.
- (64) Lucia, D. J.; Beran, P. S.; Silva, W. A. Reduced-order modeling: New approaches for computational physics. *Prog. Aerosp. Sci.* **2004**, 40, 51–117.
- (65) Nayfeh, A. H.; Younis, M. I.; Abdel-Rahman, E. M. Reducedorder models for MEMS applications. *Nonlinear Dyn* **2005**, *41*, 211–236
- (66) Decoster, M.; Van Cauwenberghe, A. A comparative study of different reduction methods. *Journal A* **1976**, *17*, 125–134.
- (67) Larsson, S.; Thomée, V. Partial differential equations with numerical methods; Springer Science & Business Media, 2008; Vol. 45.
- (68) Jaimoukha, I. M.; Kasenally, E. M. Krylov subspace methods for solving large Lyapunov equations. SIAM J. Numer. Anal 1994, 31, 227–251.
- (69) Jbilou, K.; Riquet, A. Projection methods for large Lyapunov matrix equations. *Linear. Algebra. Appl.* **2006**, *415*, 344–358.

- (70) Do, V.-N. Non-equilibrium Green function method: Theory and application in simulation of nanometer electronic devices. *Adv. Nat. Sci.: Nanosci. Nanotechnol.* **2014**, *5*, 033001.
- (71) Kadanoff, L.; Baym, G. Quantum Statistical Mechanics; WA benjamin Inc.: New York, 1962.
- (72) Caroli, C.; Combescot, R.; Nozieres, P.; Saint-James, D. Direct calculation of the tunneling current. *J. Phys. C: Solid State Phys.* **1971**, 4, 916.
- (73) Datta, S. Quantum transport: Atom to transistor; Cambridge University Press, 2005.
- (74) Popov, V. S. Tunnel and multiphoton ionization of atoms and ions in a strong laser field (Keldysh theory). *Phys.-Usp.* **2004**, *47*, 855.
- (75) Danielewicz, P. Quantum theory of nonequilibrium processes, I. Ann. Phys. 1984, 152, 239–304.
- (76) Xue, Y.; Datta, S.; Ratner, M. A. First-principles based matrix Green's function approach to molecular electronic devices: General formalism. *Chem. Phys.* **2002**, *281*, 151–170.
- (77) Meier, C.; Tannor, D. J. Non-Markovian evolution of the density operator in the presence of strong laser fields. *J. Chem. Phys.* **1999**, *111*, 3365–3376.
- (78) Sancho, M. L.; Sancho, J. L.; Rubio, J. Quick iterative scheme for the calculation of transfer matrices: application to Mo (100). *J. Phys. F: Met. Phys.* **1984**, *14*, 1205.
- (79) Sancho, M. L.; Sancho, J. L.; Sancho, J. L.; Rubio, J. Highly convergent schemes for the calculation of bulk and surface Green functions. *J. Phys. F: Met. Phys.* **1985**, *15*, 851.
- (80) Brauer, F. Perturbations of nonlinear systems of differential equations. J. Math. Anal. Appl. 1966, 14, 198–206.
- (81) Ma, L.; Li, X.; Liu, C. Coarse-graining Langevin dynamics using reduced-order techniques. *J. Comput. Phys.* **2019**, 380, 170–190.
- (82) Di Ventra, M.; Todorov, T. N. Transport in nanoscale systems: The microcanonical versus grand-canonical picture. *J. Phys.: Condens. Matter* **2004**, *16*, 8025.
- (83) Benner, P.; Gugercin, S.; Willcox, K. A survey of projection-based model reduction methods for parametric dynamical systems. *SIAM Rev.* **2015**, *57*, 483–531.
- (84) Yabana, K.; Nakatsukasa, T.; Iwata, J. I.; Bertsch, G. F. Realtime, real-space implementation of the linear response time-dependent density-functional theory. *Phys. Status Solidi B* **2006**, 243, 1121–1138.
- (85) Kurth, S.; Stefanucci, G.; Khosravi, E.; Verdozzi, C.; Gross, E. Dynamical Coulomb blockade and the derivative discontinuity of time-dependent density functional theory. *Phys. Rev. Lett.* **2010**, *104*, 236801.
- (86) Ullrich, C. A. Time-dependent density-functional theory: Concepts and applications; OUP Oxford, 2011.